Materials Science and Engineering B 176 (2011) 72–78

Contents lists available at ScienceDirect

Materials Science and Engineering B

journal homepage: www.elsevier.com/locate/mseb

Synthesis and luminescence properties of $YVO_4:Eu^{3+}$ cobblestone - like microcrystalline phosphors obtained from the mixed solvent - thermal method

Xiuzhen Xiao[a,b], Guanzhong Lu[a,b,*], Shaodian Shen[a], Dongsen Mao[a], Yun Guo[b], Yanqin Wang[b]

[a] Research Institute of Applied Catalysis, Department of Chemical Engineering, Shanghai Institute of Technology, Shanghai 200235, PR China
[b] Key Laboratory for Advanced Materials and Research Institute of Industrial Catalysis, East China University of Science and Technology, Shanghai 200237, PR China

ARTICLE INFO

Article history:
Received 10 May 2010
Received in revised form 11 August 2010
Accepted 8 September 2010

Keywords:
Vanadate
Luminescence
Mixed solvent - thermal method
Europium
Microcrystalline

ABSTRACT

The mixed solvent-thermal method has been developed for the synthesis of $YVO_4:Eu^{3+}$ luminescent materials in the N, N-dimethylformamide (DMF)/ de-ionized water (DIW) solution. The samples have been characterized by X-ray diffraction (XRD), scanning electron microscopy (SEM), transmission electronic microscope (TEM), UV/vis absorption and photoluminescence spectroscopies. The results demonstrate that we have obtained the uniform $YVO_4:Eu^{3+}$ cobblestone - like microcrystalline phosphors in the mixed solution of DMF and DIW, which are different to the as-obtained $YVO_4:Eu^{3+}$ nanoparticles in pure DIW. And the as - prepared $YVO_4:Eu^{3+}$ microcrystalline particles are composed of numerous nanoparticles. The assembling phenomenon of the nanoparticles is strongly affected by the pH value of the solution and the volume ratio of DMF/DIW. Under UV excitation, the samples can emit the bright red light. While, the photoluminescence (PL) intensities of $YVO_4:Eu^{3+}$ show some difference for samples obtained under the different reaction conditions. This is because that different microstructures of samples result in different combinative abilities between the surface and the adsorbed species so as to produce the different quenching abilities to the emission from Eu^{3+} ions.

© 2010 Elsevier B.V. All rights reserved.

1. Introduction

Rare earth luminescent materials have considerable practical applications in almost all devices involving the artificial light sources, such as cathode ray tubes, lamps and X-ray detectors, etc.[1–7]. As for a host, yttrium vanadate (YVO_4) has been shown to be a useful host lattice for rare earth ions to produce phosphors emitting a variety of colors since high luminescence quantum yields are observed for the f–f transitions [8–10]. The main work during the past focused on the Eu^{3+}-activated YVO_4, because it was an important commercial red-emitting phosphors used in color television, the cathode ray tube, and the high-pressure mercury lamp [11]. And it was firstly introduced by Levine and Pallia as red primary in color television in 1964 [12].

It was well known that the grain size, morphology, agglomeration, or surface passivation have a great influence on the properties of phosphor [13]. The quantum yield of the nanophosphors is usually lower than that of bulky phosphors and bulk $YVO_4:Eu^{3+}$ phosphor has a high photoluminescent (PL) quantum yield of about 70% [14]. In most cases, bulky $YVO_4:Eu^{3+}$ is synthesized by solid - state reaction at temperatures above 1200 K [15–17]. However, there exist two serious drawbacks: first, high temperature and considerable time were required because of the low reactivity of the oxides involved and the slow diffusion rates. Moreover, it provides agglomerated powders with a grain size in the 5–20 μm range. To overcome these limitations, solution-based chemical methods, including hydrothermal synthesis [18–20], hydrolyzed colloidal reaction (HCR) technique [21], *in situ* precipitation [22], the combustion solution process [23], the polyacrylamide gel method [24], and the spray freeze-drying process [25], have been developed to prepared YVO_4 doped with luminescent activators. Among them, the hydrothermal method is the most promising solution techniques for preparation of YVO_4 powders with controlled shape and size. For examples, Wu et al. tailored the size and shape of YVO_4 crystallites by changing the reaction condition such as yttrium–to–vanadium ratio, pH value, reaction temperature and time, and organic molecules additives [26]. Wu et al. controlled the synthesis of rodlike, olivelike and pineapplekike nanocrystals of the YVO_4:Eu by using porous silicon substrates, V_2O_5 nanowires, and CTAB additives at pH 6–7 [27]. Xu et al. fabricated the nano - and micro - scaled Eu-doped YVO_4 powders via Na_2EDTA-assisted hydrothermal process in a wide pH range at 180 °C for 24 h [28].

The solvothermal process is an extension of the hydrothermal method, in which chemical reactions are carried out in an autoclave in the presence of a nonaqueous solvent above room temperature and at elevated pressure. To the best of our knowledge,

* Corresponding author at: Research Institute of Applied Catalysis, Department of Chemical Engineering, Shanghai Institute of Technology, Shanghai 200235, P R China. Tel.: +86 21 64252923; fax: +86 21 64253703.
E-mail address: gzhlu@ecust.edu.cn (G. Lu).

0921-5107/$ – see front matter © 2010 Elsevier B.V. All rights reserved.
doi:10.1016/j.mseb.2010.09.005

solvothermal reaction in a homogeneous mixed solution has been proven to be a convenient way to control the morphology and phase structure of resulting products by adjusting the composition of the mixed solution. In most cases, this method was widely applied in the fabrication of the semiconductor nanocrystals [29–32]. While, the report on the solvothermal synthesis of YVO_4 luminescent material is still few. Kakihana et al. used methanol–water mixed solvent as a reaction medium to prepare YVO_4:Eu^{3+} phosphor materials and spherical particles were obtained at lower temperatures, consisted of chains composed of ~ 10 nm; however, at above the critical temperature, the powders have a raspberry shape [33]. Although thermodynamics provide an unambiguous description of such mixed solvent systems, very little is known about the molecular structures of solvents during the elevated reaction temperature, and the process may benefit from unique molecular arrangements of the solvent molecules and solvated ions for the synthesis of solid - state materials. In this work, we adopted a DMF–DIW solvent as the reaction medium to synthesize the YVO_4:Eu^{3+} luminescent materials via a solvothermal method. Furthermore, we have also investigated the influence of the solvent volume ratio of DMF to DIW on the internal structure of the powders, which will affect the luminescence properties of Eu^{3+}.

2. Experimental

2.1. Synthesis of YVO_4:Eu^{3+} luminescent material with cobblestone-like micro-scaled morphology

All chemicals were purchased from Shanghai Chemical Reagents Company and used without further purification. The synthesis of YVO_4:Eu^{3+} powders can be described as follows: Eu_2O_3 was firstly reacted with concentrated nitric acid, and a appropriate volume of de-ionized water was added to form a 0.02 M $Eu(NO_3)_3$ aqueous solution. 1 mmol NH_4VO_3 was dissolved in dilute nitric acid. Subsequently, appropriate volume of the $Eu(NO_3)_3$ solution and appropriate amounts of $Y(NO_3)_3{\cdot}6H_2O$ were added to the above NH_4VO_3 aqueous solution. Then DMF solvent was added into the solution and the volume ratio of DMF/DIW was 0, 1/7, 1 and 3, respectively. At the same time, the pH value of the resultant solution was adjusted to be 5 by ammonia. After stirring for 5 h, this synthesis solution was poured into a Teflon lined stainless steel autoclave. The autoclave was sealed and maintained at 160 °C for 3 days and then cooled to room temperature. The resultant product was filtered, washed with de-ionized water and absolute alcohol to remove ions possibly remaining in the final products, and finally dried at 80 °C in air for further characterization.

Other samples were prepared by the similar procedure except the different pH values of the mixture, which were adjusted to be 2 and 11, respectively, by adding ammonia or HNO_3. And the volume ratio of DMF/DIW was fixed to be 1. All samples are denoted successively as a, b, c, d, e, and f, respectively, in the following description (samples a–d were obtained under the volume ratio of DMF to DIW is 0, 1/7, 1, and 3, respectively; samples e and f obtained under the pH value of 2 and 11, respectively).

In this synthetic process, organic DMF and DIW have been used as solvents and the volume ratio of DMF to DIW has been adjusted to modify the microstructure of the products. YVO_4:Eu^{3+} microparticles have been obtained via this solvo-hydrothermal method. For micro-scaled phosphors, three-dimensional sizes of crystalline grain are very thick to afford high strength, which would be very useful for the application to obtain high efficient phosphors [29].

2.2. Characterization

The samples to be measured were firstly ground to be powders, and then smeared on to a zero-diffraction quartz plate. Step-scan X-ray powder-diffraction data were collected over the 2θ range 10–80° with CuKα radiation (λ = 1.540598 Å; 40 kV, 40 mA) on an X' Pert PRO X-ray diffractometer. The scanning electron microscopic (SEM) images were obtained on a HITACHI S-3400N. The samples were coated with a thin layer of gold (Au coating) using an Hitachi Ions Sputter coater E-1010 to prevent sample charging prior to analysis and allow quality image observation and recording. Transmission electron microscopy (TEM) images were obtained on a JEOL JEM-2100 microscope operated at 200 kV and the sample to be measured was first dispersed in ethanol and then collected using copper grids covered with carbon film. The excitation and emission spectra of samples were recorded on a Cary Eclipse fluorescence spectrophotometer (Varian) equipped with a 150 W xenon lamp as the excitation source. UV–vis absorption spectra of dry pressed samples were obtained on a Cary 100 Bio UV–vis spectrophotometer (Varian) and $BaSO_4$ was used as a reference standard. The diffuse-reflectance data was converted to the absorption data using Kubela–Munk function. All the measurements were performed at room temperature.

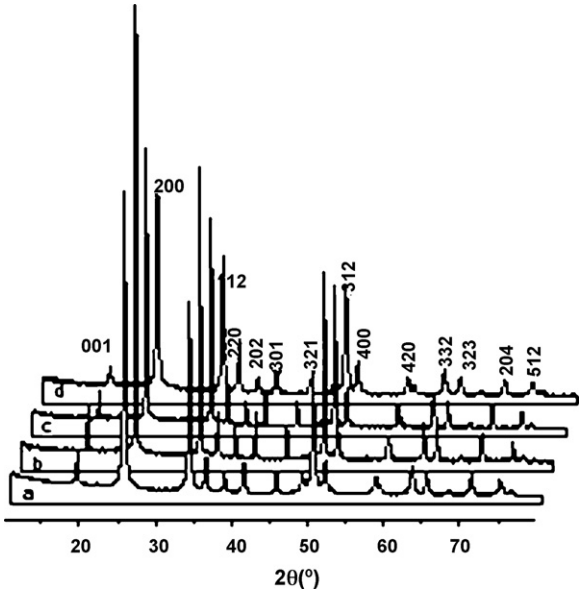

Fig. 1. XRD patterns of YVO_4:5%Eu^{3+} prepared in the mixed solvents of DMF and DIW with the different volume ratios of V_{DMF}/V_{DIW}: (a) sample a, (b) sample b, (c) sample c, and (d) sample d.

3. Results and discussions

3.1. Morphology and structure of YVO_4:Eu^{3+}

3.1.1. The influence of the volume ratio of DMF/DIW

XRD patterns of samples a, b, c, and d correspond, respectively, to Fig. 1(a)–(d), which can be indexed as a pure tetragonal phase, approaching the standard values for the bulk YVO_4 (JCPDS card 72-0861). The results show that the crystalline phases of as-prepared YVO_4 in the mixed DMF–DIW solvent are similar to that of YVO_4 nanoparticles in the pure DIW. The lattice parameters were calculated using the following relationship between Bragg diffraction spacing and tetragonal cell parameters, which were given in Table 1.

$$\frac{1}{d_{hkl}^2} = \frac{h^2 + k^2}{a^2} + \frac{l^2}{c^2}$$

where d_{hkl} is the Bragg diffraction spacing for the ($h\,k\,l$) plane and $h\,k\,l$ are miller indices a and c are cell parameters.

Table 1
.Lattice parameters of YVO_4:5%Eu^{3+}prepared via. the solvothermal method under the different reaction conditions.

No. of samples	*a* (Å)	*c* (Å)
JCPDS 72-0861	7.123	6.292
Sample a	7.126	6.304
Sample b	7.122	6.329
Sample c	7.118	6.288
Sample d	7.104	6.363
Sample e	7.168	6.241
Sample f	7.118	6.288

Scanning electron microscopic was used to examine the as - prepared samples via the solvo-thermal method under the mixed solvent of DMF to DIW. The representative SEM pictures of samples b, c, and d have been shown in Fig. 2(a)–(c). A number of cobblestone - like micro-scaled particles can be clearly observed. In order to investigate their internal structure, as-prepared samples have been further characterized by transmission electron microscopy (TEM). Fig. 3 shows the TEM images of samples a, b, c, and d, respectively. As shown in Fig. 3, the microstructure of samples presents some differences. From Fig. 3(a), sample a which prepared only using the DIW solvent presents well dispersed nanoparticles of 20–40 nm. While, with the addition of DMF solvent, as-prepared samples b, c and d show microparticles assembled by numerous of nanoparticles. Furthermore, it can be found that the increase in the volume of DMF reduce interspace between two nanoparticles which aggregated to microparticles. In the central section of a single cobblestone - like YVO_4 microparticles (Fig. 3(c) and (d)), the fringe of nanoparticles is not observed clearly; especially for sample d prepared in the mixed solvent of V_{DMF}/V_{DIW} = 3/1, it is very difficult to see the assembling of nanoparticles, but we still can prove that this cobblestone - like morphology was formed by gathering of nanoparticles from the high-magnification TEM image in Fig. 3(e), which is taken from the fringe of a microscaled particle marked with a red rectangle in Fig. 3(d). As seen in Fig. 3(e), the nanoparticles in the YVO_4:Eu^{3+} (5%) microcrystal can be clearly seen.

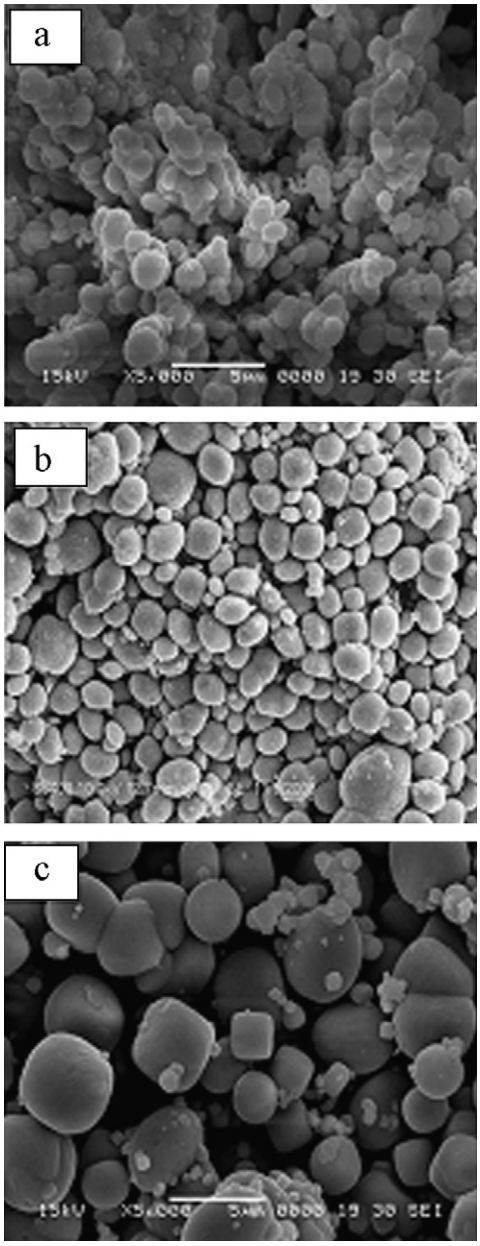

Fig. 2. SEM images of YVO_4:5%Eu^{3+} prepared in the mixed solvents of DMF and DIW with the different volume ratios of V_{DMF}/V_{DIW}: (a) sample b, (b) sample c, and (c) sample d.

It was well known that the control in the particle size and morphologies not only depends on the inherent structural characteristics of the compounds but also on experimental conditions, such as the reaction time, reaction temperature, surfactants, and solvents. According to the experimental results mentioned above, the possible growth mechanism or evolution of microscaled YVO_4 materials may be described as follows: first, the direct mixing of two solutions containing metal Y^{3+} and $V_3O_9{}^{3-}$ ($Y^{3+} + V_3O_9{}^{3-} + Eu^{3+} \rightarrow YVO_4$:$Eu^{3+}$)[34] produces a large number of YVO_4 nuclei rapidly under a mixed solvent - thermal condition; then the nuclei begin to aggregate in a random way, which is probably due to the presence of the organic solvent DMF, and finally the cobblestone-like microcrystal YVO_4 are formed gradually. When the DMF volume is low, the microcrystal YVO_4 remained a little loose and contained numerous nanoparticles. When the volume of DMF is increased, we got YVO_4:Eu^{3+} microcrystal with compact structure. These results clearly confirmed that the volume of DMF used here could affect the microstructure of as - obtained YVO_4:Eu^{3+}. It can be seen that DMF not only strongly adsorbed on the surface of the nanoparticles, controlling them to grow into uniform nanoparticles serving as building blocks, but also profoundly influence the assembly these building blocks by interaction force [35,36].

3.1.2. The influence of pH value

The pH value in synthetic system plays an important role in the preparation of YVO_4:Eu^{3+} by a hydrothermal method. Tuning the pH value of synthesis solution can modulate the thermodynamics/kinetics of nucleation and growth of the nanoparticles by controlling experimentally the interfacial tension (surface free energy), resulting in the changes of the structure and morphology of the final products. The XRD patterns of samples e, c and f synthesized in the mixed solvents of DMF and DIW (V_{DMF}/V_{DIW} = 1) at the pH value of 2, 5, 11, respectively, are shown in Fig. 4. The diffraction peaks in all patterns have the similar features and belong to the tetragonal phase of bulk YVO_4, and however the intensities of the peaks are different for the different samples. With a decrease in the pH value, the diffraction peaks become sharp and their intensity become strong, indicating that the prepared products have better crystallinity and the bigger particle size.

The SEM and TEM images of samples e, c and f synthesized in the mixed solvents of DMF and DIW (V_{DMF}/V_{DIW} = 1) at the pH value of 2, 5, 11, respectively, are shown in Fig. 5. As-prepared YVO_4:Eu^{3+} (5%) at pH 2 presents the cobblestone - like morphology with diameter of 1–2 μm (Fig. 5(a)), and we cannot see the assembling of nanoparctiles (Fig. 5(b)). When the pH value of synthesis solution was 5 or

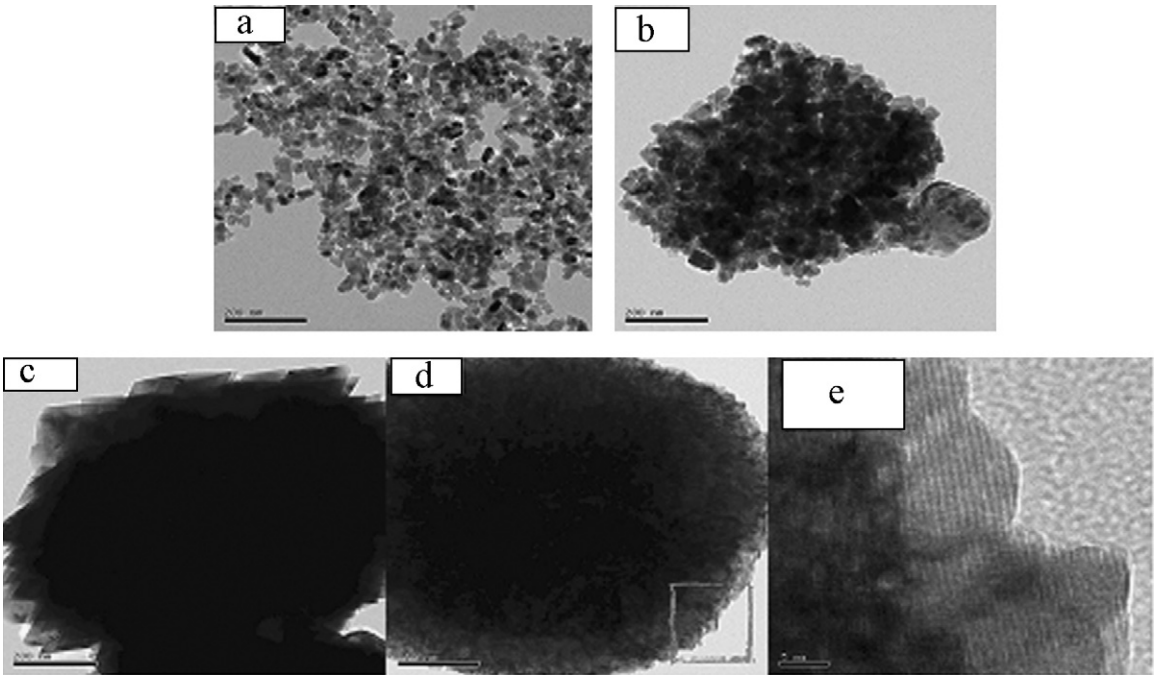

Fig. 3. TEM images of YVO_4:5%Eu^{3+} prepared in the mixed solvents of DMF and DIW with the different volume ratios of V_{DMF}/V_{DIW}: (a) sample a, (b) sample b, (c) sample c, (d) sample d, and (e) the high-magnification TEM image of sample d.

11, the morphologies of the YVO_4:Eu^{3+} (5%) prepared was quite different from the sample synthesized at pH 2. The as-prepared sample at pH 5 is also microscaled cobblestone–like particle with diameter in the interval of 0.5–1 μm (Fig. 5(c)), and its TEM image in Fig. 5(d) shows that, it is composed of numerous nanoparticles. Fig. 5(e) and (f) shows the SEM and TEM images of the YVO_4:Eu^{3+} (5%) prepared at pH 11. The results show that, these as-synthesized powders with the size of 0.15–0.2 μm consist of several nanoparticles with the particle size of 20–30 nm. Obviously, the assembling of nanoparticles has been affected by the pH value of the synthesis solution (V_{DMF}/V_{DIW} = 1). Since the forms of vanadium ions are extremely sensitive to the pH of the solution [33], the vanadium ions would exist as VO^{2+} ions when the solution is of strong acidity; when pH rises to 2, vanadium ions exist in the form of $V_{10}O_{28}{}^{6-}$ principally; when pH 5, vanadium ions are liable to the form of $V_3O_9{}^{3-}$ when the pH value is in range of 7–11, the $VO_4{}^{3-}$ ions has been dominant. The studies of Li [37] and Su [38] show that the presence of $VO_4{}^{3-}$ benefits the formation of larger particles. Herein, the contrary result has been obtained, that is, with an increase in pH value of synthesis solution, the particle size of prepared sample decreases. Different from the synthesis conditions reported by Li, we adopt the mixed solvents of DMF and DIW rather than the pure DIW to prepare YVO_4:Eu^{3+}. DMF is an aprotogenic solvent comparing with DIW and can affects the environment of hydrothermal process for the crystalline growth.

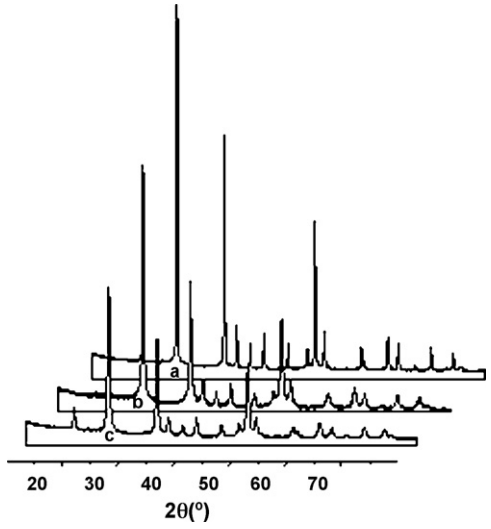

Fig. 4. XRD patterns of YVO_4:5%Eu^{3+} in the mixed solvents (V_{DMF}/V_{DIW} = 1) at pH value of (a) sample e, (b) sample c, and (c) sample f.

3.2. UV–vis absorption spectroscopies

Fig. 6(a)–(d) presents the UV–vis spectra of samples a, b, c and d, prepared via the mixed solvent-thermal method (pH 5) with different solvent ratio (V_{DMF}/V_{DIW}), and there are the absorption peaks at 295, 310, 315, and 330 nm. Fig. 6(d)–(f) shows the UV–vis spectra of samples c, e and f, obtained with different pH values (V_{DMF}/V_{DIW} = 1) and the absorption bands are located at 325, 315 and 308. It is reported that the peak of the absorption band for YVO_4: Eu^{3+} nanoparticles (in sizes ranging from 36 to 53 nm) is 272 nm, which can be assigned to the $^1a_1 \rightarrow {}^1t_1$ ($t_1 \rightarrow 2e$) transition of $VO_4{}^{3-}$ ions [39]. Generally, the $^1a_1 \rightarrow {}^1t_1$ ($t_1 \rightarrow 2e$) is forbidden, as the size of the particles decrease and the deformation of the structure increases, $^1a_1 \rightarrow {}^1t_1$ can be partly allowed [27,40,41], however, in our experiment, the powders present the micro–sized particles, which are composed of a large number of nanoparticles and behave possibly the feature of micrometer- and nanometer-scaled particles. In the UV–vis spectra, the absorption peaks of these samples shift to the lower energy in the UV region and are attributed to the charge transfer from the oxygen ligands to the central vanadium atom inside the $VO_4{}^{3-}$ anionic and europium ions [42–44].

3.3. Photoluminescence characterization

Taken at an emission wavelength of 613 nm, the excitation spectra of all YVO_4:Eu^{3+}(5 mol%) were obtained, which fit well with the absorption spectra. As shown in Fig. 7(a)–(f), they consist of a broad

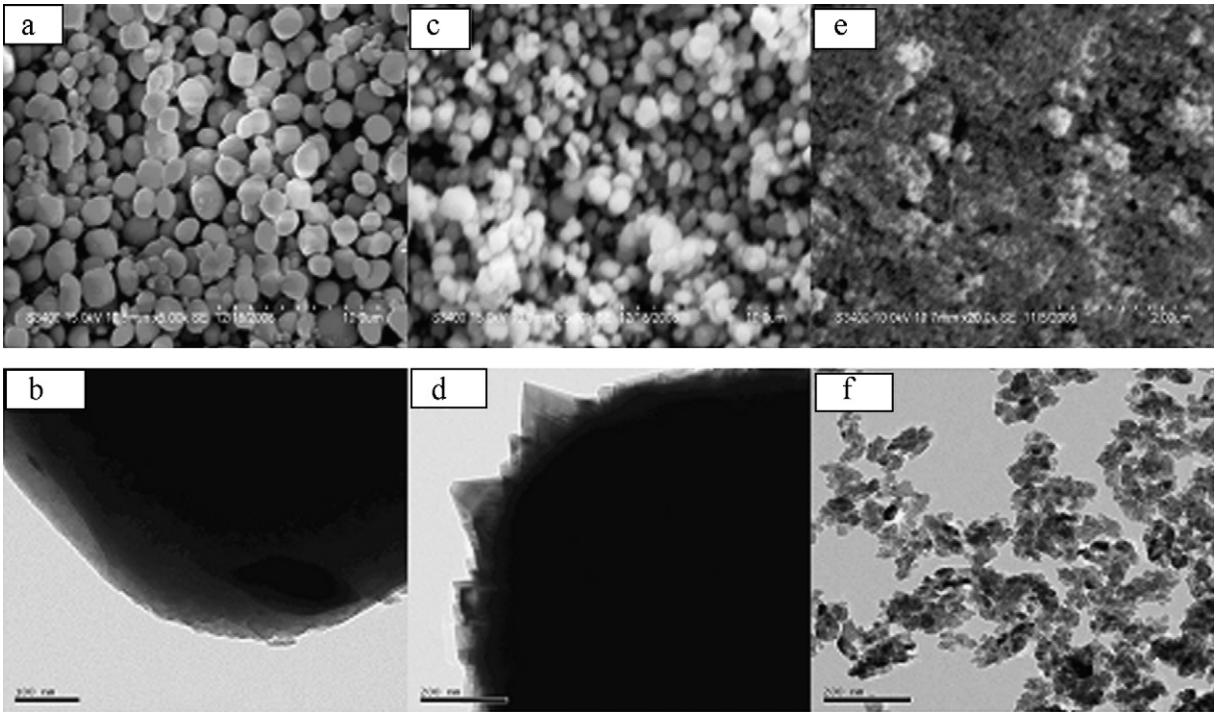

Fig. 5. SEM (a, c, e) and TEM (b, d, f) images of as-prepared YVO_4:5%Eu^{3+} in the mixed solvents (V_{DMF}/V_{DIW} = 1) at pH value of (a) and (b) sample e, (c and d) sample c and (e and f) sample f.

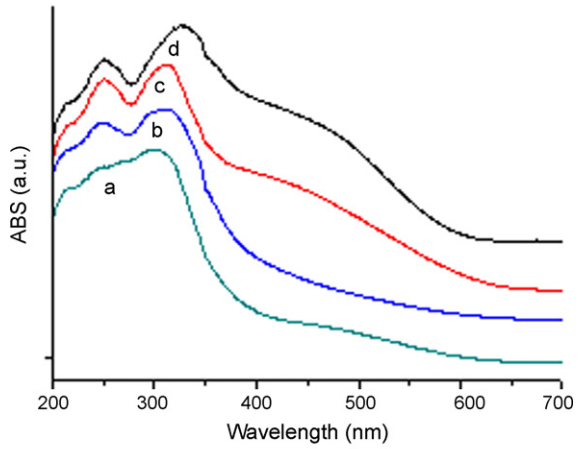

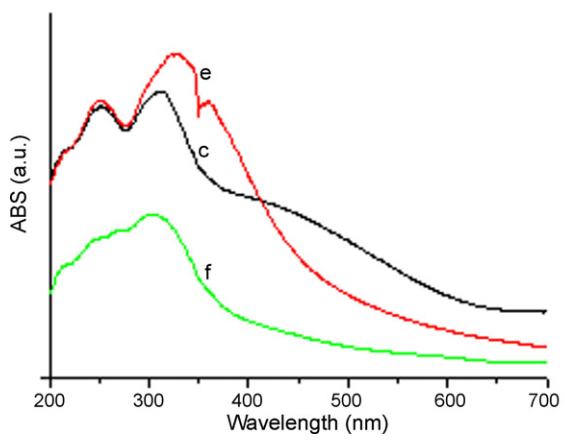

Fig. 6. UV–vis spectra of YVO_4:5%Eu^{3+} in the mixed solvents (pH 5) of DMF and DIW with different volume ratio: (a) sample a, (b) sample b, (c) sample c, (d) sample d; and in the mixed solvents of V_{DMF}/V_{DIW} = 1 with different pH value: (e) sample e, (c) sample c, and (f) sample f.

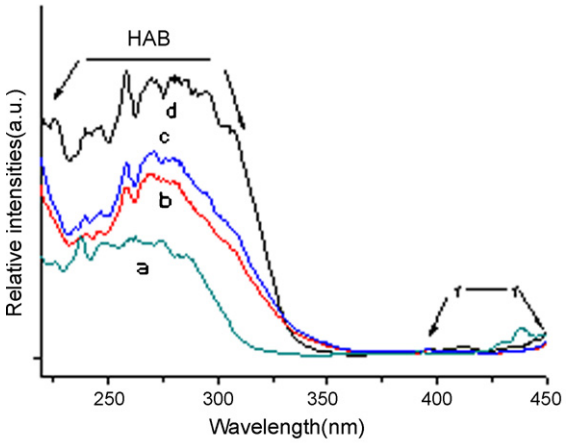

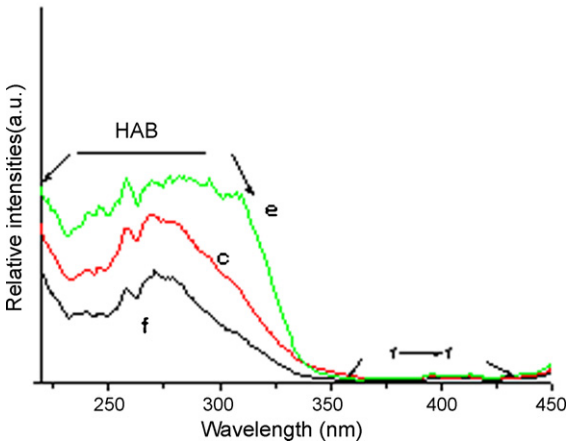

Fig. 7. Excitation spectra of YVO_4:5%Eu^{3+} in the mixed solvents (pH 5) of DMF and DIW with different volume ratio: (a) sample a, (b) sample b, (c) sample c, (d) sample d; and in the mixed solvents of V_{DMF}/V_{DIW} = 1 with different pH value: (e) sample e, (c) sample c, and (f) sample f.

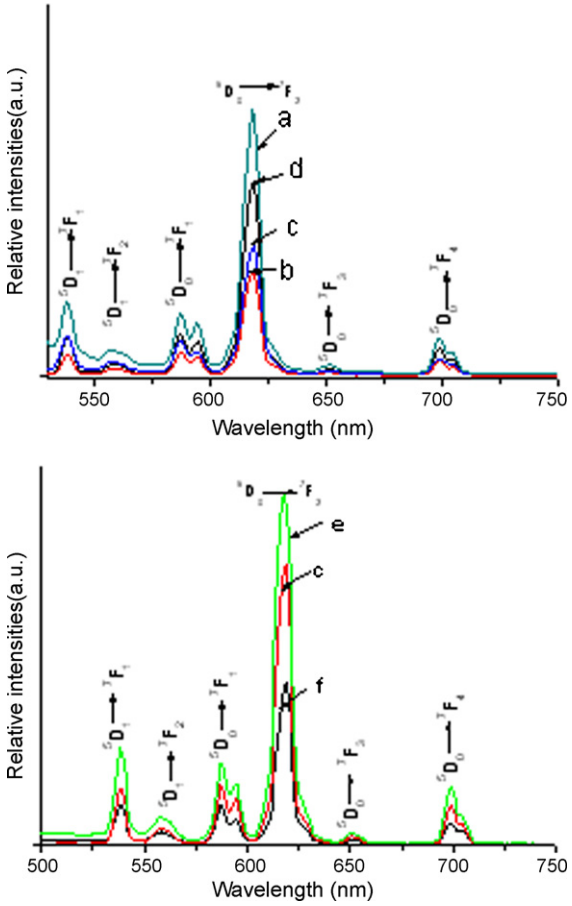

Fig. 8. Emission spectra of YVO_4:5%Eu^{3+} in the mixed solvents (pH 5) of DMF and DIW with different volume ratio: (a) sample a, (b) sample b, (c) sample c, and (d) sample d; and in the mixed solvents of V_{DMF}/V_{DIW} = 1 with different pH value: (e) sample e, (c) sample c, and (f) sample f.

band in the ultraviolet range of 200–300 nm and several sharp lines in the range of 300–500 nm. The broad band is ascribed to the charge transfer stated originating from the oxygen ligands to the central vanadium atom inside the VO_4^{3-} ion, confirming that the emission occurs after energy transfer from the excited vanadate to the europium ions. The weak absorption in the longer wavelength region originates from the general f–f transitions within the Eu^{3+} $4f^6$ electronic configuration, which position cannot be changed in different hosts due to the shielding of the 4f electrons by outer shell 5s and 5p electrons.

The emission spectra of Eu^{3+} (5 mol%)-activated samples prepared at different conditions are presented in Fig. 8. All the spectra contains the characteristic transition lines from the lowest excited $^5D_0$. The assignments for the main emission lines of Eu^{3+} are labeled in the figure. Obviously, the emission spectra are dominated by the red $^5d_0 \rightarrow {}^7f_2$ hypersensitive transition of Eu^{3+}, indicating the absence of an inversion symmetry at the Eu^{3+} lattice site in the YVO_4 host lattices [45]. YVO_4 belongs to a tetragonal structure with a space group of I41/amd, which is composed of YO_8 dodecahedra (the point symmetry of Y^{3+} is D_{2d} without an inversion center) and VO_4 tetrahedral (T_{2d}). The Eu^{3+} occupy the Y^{3+} sites in the YVO_4 particles, as a result, the hypersensitive transitions are the most prominent group in their emission spectra [46]. The red emission ($^5D_0 \rightarrow {}^7F_2$ at ca. 610 nm) in Eu^{3+}-activated YVO_4 is predominant over the orange emissions ($^5D_0 \rightarrow {}^7F_1$ at ca. 590 nm), which is important for a red phosphor. Other contributions of weaker importance are the $^5D_0 \rightarrow {}^7F_{1,3}$ magnetic dipole transitions. In the emission spectra (Fig. 8), not only the characteristic transition lines from the lowest excited $^5D_0$ level of Eu^{3+} are observed, but also those from higher energy levels ($^5D_1$, $^5D_2$ and $^5D_3$) of Eu^{3+} are detected. The presence of emission lines from higher excited states of Eu^{3+} ($^5D_1$, $^5D_2$ and $^5D_3$) is attributed to the low vibration energy of VO_4^{3-} groups (823 cm^{-1}). The multiphonon relaxation of VO_4^{3-} is not able completely to bridge the gaps between the higher energy levels ($^5D1$, $^5D_2$ and $^5D_3$) and $^5D_0$ level of Eu^{3+}, resulting in the weak emission from these levels [11].

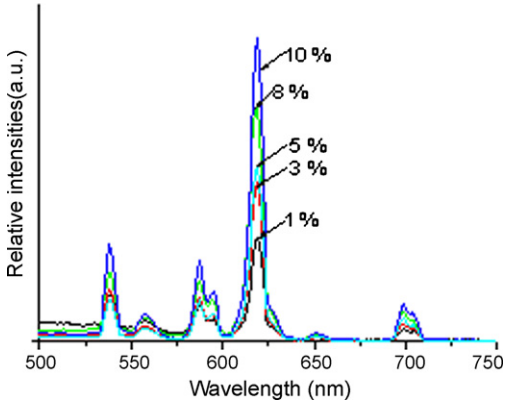

Fig. 9. Emission spectra of as-prepared YVO_4:x%Eu^{3+} (x = 1, 3, 5, 8, 10) in the mixed solvents (pH 5) of 1. V_{DMF}/V_{DIW} = 1.

From Fig. 8(a), the luminescent intensity of sample a prepared in DIW is the strongest one among all samples. While among samples b, c and d, sample d presents the strongest luminescence intensity and sample c show stronger one than sample b. According to the literatures [27,28], the difference of PL intensity of the samples may be caused by the different quenching abilities of the adsorbed species on the surface to the emission from Eu^{3+} ions. For sample a, which prepared in DIW, its surface can be only covered with hydroxyl species; while, for samples b, c, and d, which prepared in the mixed solvent of DMF and DIW, their surfaces may be adsorbed both hydroxyl species and DMF. Hydroxyl species and DMF may be acted as the quencher of the excited Eu^{3+} ions. So sample a prepared in DIW present the strongest PL intensity. At the same time, the difference of PL intensity for samples b, c and d may be attributed to their different shapes and sizes, which also can be used to explain the difference of PL intensity for samples c, e and f. It has been reported that the combinative abilities between quenching species and crystal surfaces is affected by the sizes and shapes of YVO_4 [24], so changing the morphology of powders, luminescence properties can be effectively tuned.

The emission spectra of YVO_4:x%Eu^{3+} (x = 1, 3, 5, 8, 10) microcrystalline phosphors with different doping concentrations were also investigated, which was synthesized by the mixed solvent–thermal method at pH 5 and V_{DMF}/V_{DIW} = 1. As shown in Fig. 9, it can be seen clearly that the concentration quenching of activator appears at high concentration of Eu^{3+} when the phosphor particles were excited by UV light. There is a maximum at a doping level of about 8% europium ions, and then its intensity slowly decreases with increasing further the concentration of europium ions. This partial quenching of the luminescence at high europium concentrations is a typical property of lanthanide-doped systems.

4. Conclusions

In summary, a DMF–DIW mixed solvent was used for the solvothermal synthesis of YVO_4:Eu red phosphor. In comparison with YVO_4:Eu nanoparticles prepared in DIW, as-prepared samples show micronmeter dimension and are composed of numerous nanoparticles, indicating the DMF–DIW mixed solvent can be

adopted to tailor the morphology of YVO_4:Eu. Furthermore, the internal structure of YVO_4: Eu microparticles is different for samples obtained under the different reaction conditions. When V_{DMF}/V_{DIW} is high or the solution is strongly acidic, nanoparticles aggregated closely to form the microparticles and the interspace between two nanoparticles in the center of microparticles cannot be seen. However, when V_{DMF}/V_{DIW} is low or the solution is strongly basic, nanoparticles assembled loosely to form the microparticles and the interspace between two nanoparticles in the center of microparticles can be seen clearly. Photoluminescence measurements showed that the relative intensity changed with the internal structure of the microparticles. The PL intensity of YVO_4:Eu microparticles assembled closely by nanoparticles is the strongest one among these samples.

Acknowledgments

This study was supported financially by the National Basic Research Program of China (2010CB732300), International Science and Technology Cooperation Program of China (2006DFA42740), the National Natural Science Foundation of China (20601008), the Education Committee of Shanghai (J51503).

References

[1] G.B. Blasse, C. Grabmeter, Luminescent Materials, Springer Verlag, Berlin, 1994.
[2] K. Riwotzki, M. Haase, J. Phys. Chem. B 105 (2001) 12712.
[3] O. Chukova, S.Z. Nedilko, M. Pashkovskyi, J. Lumin. 102–103 (2003) 498.
[4] H.F. Brito, O.L. Malta, M.C.F.C. Felinto, J. Alloy Compd. 344 (2002) 293.
[5] R. Reisfeld, M. Zelner, A. Patra, J. Alloy Compd. 300–301 (2000) 147.
[6] H.J. Zhang, J.Y. Wang, C.Q. Wang, L. Zhu, X.B. Hu, X.L. Meng, M.H. Jiang, Y.T. Chow, Opt. Mater. 23 (2003) 449.
[7] R.X. Yan, X.M. Sun, X. Wang, Q. Peng, Y.D. Li, Chem. Euro. J. 11 (2005) 2183.
[8] R. Kubo, J. Phys. Soc. Jpn. 17 (1962) 975.
[9] G. Mills, L. Zongguan, D. Meisel, J. Phys. Chem. 92 (1988) 822.
[10] M. Yu, J. Lin, J. Fang, Chem. Mater. 17 (2005) 1783.
[11] M. Yu, J. Lin, Z. Wang, J. Fu, S. Wang, H.J. Zhang, Y.C. Han, Chem. Mater. 14 (2002) 2224.
[12] F.M. Nirwan, T.K. Gundu Rao, P.K. Gupta, R.B. Pode, Phys. Stat. Sol. (a) 198 (2003) 447.
[13] M. Bredol, U. Kynast, C. Ronda, Adv. Mater. 7/8 (1991) 361.
[14] W.L. Wanmaker, A. Bril, W. ter Vrugt, J. Broos, Philips Rep. 21 (1966) 270.
[15] B. Yan, X.Q. Su, K. Zhou, Mater. Res. Bull. 41 (2006) 134.
[16] K.S. Shim, H.K. Yang, B.K. Moon, B.C. Choi, J.H. Jeong, J.H. Kim, J.S. Bae, K.H. Kim., Curr. Appl. Phys. 9 (2009) S226.
[17] G.H. Pan, H.W. Song, Q. Dai, R.F. Qin, X. Bai, B. Dong, L. Fan, F. Wang, J. Appl. Phys. 104 (2008) 084910.
[18] X.C. Wu, Y.R. Tao, C.J. Mao, D.J. Liu, Y.Q. Mao, J. Cryst. Growth 290 (2006) 207.
[19] G.H. Pan, H.W. Song, X. Bai, L.B. Fan, H.Q. Yu, Q.L. Dai, B.L. Dong, R.F. Qin, S.W. Li, S.Z. Lu, X.G. Ren, H.F. Zhao, J. Phys. Chem. C 111 (2007) 12472.
[20] L. Chen, Y. Liu, K. Huang, Mater. Res. Bull. 4 (2006) 158.
[21] S. Erdei, N.M. Rodriguez, F.W. Ainger, W.B. White, D. Ravichandran, L.E. Cross, J. Mater. Chem. 8 (1998) 99.
[22] B. Yan, X.Q. Su, K. Zhou, Mater. Res. Bull. 4 (2006) 134.
[23] S. Ekambaram, K.C. Patil, J. Alloy Compd. 217 (1995) 104.
[24] H. Zhang, X. Fu, S. Niu, G. Sun, Q. Xin, J. Solid State Chem. 177 (2004) 2649.
[25] M. Iwamura, V. Petrykin, M. Kakihana, J. Ceram. Soc. Jpn. 115 (2007) 920.
[26] H. Wu, H. Xu, Q. Su, T. Chen, M. Wu, J. Mater. Chem. 13 (2003) 1223.
[27] X. Wu, Y. Tao, C. Song, C. Mao, L. Dong, J. Zhu, J. Phys. Chem. B 110 (2006) 15791.
[28] J. Wang, Y.H. Xu, M. Hojamberdiev, J.H. Peng, G.Q. Zhu, Mater. Sci. Eng. B 156 (2009) 42.
[29] S.L. Xiong, J. Shen, M.Q. Xie, Y.Q. Gao, Q. Tang, Y.T. Qian, Adv. Funct. Mater. 15 (2005) 1787.
[30] Q. Peng, Y.J. Dong, Z.X. Deng, Y.D. Li, Inorg. Chem. 41 (2002) 5249.
[31] W.T. Yao, S.H. Yu, Q.S. Wu, Adv. Funct. Mater. 17 (2007) 623.
[32] X.J. Chen, H.F. Xu, N.S. Xu, F.H. Zhao, W.J. Lin, G. Lin, Y.L. Fu, Z.L. Huang, M.M. Wang, Wu, Inorg. Chem. 42 (2003) 3100.
[33] K.P. Sulawan, N. Kouichi, P. Valery, T. Somchai, K. Masato, J. Am. Ceram. Soc. 92 (2009) S16.
[34] G. Li, S. Pang, Z. Wang, H. Peng, Z. Zhang, Eur. J. Inorg. Chem. (2005), 2060.
[35] Y. Li, M.H. Cao, L.Y. Feng, Langmuir 25 (3) (2009) 1705.
[36] Q. Zhao, Y. Xie, Z. Zhang, X. Bai, Cryst. Growth Des. 7 (2007) 153.
[37] G.C. Li, K. Chao, H.R. Peng, K.Z. Chen, J. Phys. Chem. C 112 (2008) 6228.
[38] L.D. Su, Y.X. Zhang, J. Zhang, C.H. Yan, C.H. Liao, C.S. Lu, Y.Q. Lu, Solid State Commun. 124 (2002) 35.
[39] K. Riwotzki, M. Haase, J. Phys. Chem. B 102 (1998) 10129.
[40] H. Kubo, G. Blass, J. Inorg. Nucl. Chem. 40 (1978) 215.
[41] G. Blass, Struct. Bonding 42 (1980) 1.
[42] Y.S. Chang, F.M. Huang, Y.Y. Tsai, L.G. Teoh, J. Lumin. 129 (2009) 1181.
[43] H. Zhang, X. Fu, S. Niu, G. Sun, Q. Xin, Solid State Commum. 132 (2004) 527.
[44] M. Yun, W. Zhang, S. Xia, J.C. Krupa, J. Lumin. 68 (1996) 335.
[45] A. Huignard, T. Gacoin, J.P. Boilot, Chem. Mater. 12 (2000) 1090.
[46] A. Huignard, V. Buissette, A. Franville, T. Gacoin, J. Boilot, J. Phys. Chem. B 107 (2003) 6754.